

Distributed aggregation control of grid-interactive smart buildings for power system frequency support

Yu Wang, Yan Xu, Yi Tang*

School of Electrical and Electronic Engineering, Nanyang Technological University, 50 Nanyang Avenue, 639798 Singapore, Singapore

HIGHLIGHTS

- A new distributed aggregation method of grid-interactive smart buildings.
- Fast system frequency support by the building aggregators.
- Aggregator power tracking and energy recovery based on frequency deviation.
- Fair power and energy sharing among all participated buildings.
- Validation of the proposed method in a three-area power system with renewable energy.

ARTICLE INFO

Keywords:

Grid-interactive smart buildings
Power and energy sharing
Distributed sliding mode control
Demand response
Frequency regulation

ABSTRACT

Grid-interactive smart buildings with thermostatically-controlled loads can be modeled as virtual energy storage systems with dissipation, which have great potentials for providing grid ancillary services such as frequency support. In this paper, a new distributed aggregation control method is proposed for multiple grid-interactive smart buildings in one frequency control area (e.g. a residential community) to provide fast frequency support. The proposed method is based on the distributed sliding mode control via a leader-follower communication scheme. A leader control is designed to provide power and comfort/energy level references for the smart building aggregator based on the area frequency deviation, while references are tracked by each smart building using the proposed distributed sliding mode control. The stability of the proposed control method for grid-interactive smart buildings is proved by the Lyapunov method. With the proposed method, the external characteristics of the aggregated smart buildings will have good power tracking and energy recovery capability, which can effectively improve the system frequency response. In the aggregator, fair and efficient power and comfort/energy level sharing are achieved among all participating grid-interactive smart buildings. The proposed control scheme is tested on a three-area power system considering both system contingency and normal operation scenarios.

1. Introduction

1.1. Background and motivation

In the last decade, the penetration of renewable energy resources into modern power systems is increasing rapidly. For example, in Singapore, the projected photovoltaics (PVs) generation will be increased to 350 MWp by 2020 [1]. However, high penetrations of renewable energy sources (RESs) such as solar PV and wind power have reduced power system inertia by replacing the synchronous machines [2], which can significantly challenge the system frequency regulation [3], control schemes [4] and transient stability [5]. In the meantime,

fast and stochastic power variations of RESs will also lead to rapid frequency fluctuations [6]. It is well known that the power system frequency is an indicator of real-time power balancing between generation and consumption. So the frequency regulation becomes quite important in order to maintain a stable and efficient operation of the power systems. The severe frequency deviations can lead to load/generation trip-off, which jeopardize the stability and security of power systems as well as decline energy efficiency. A possible way to deal with the negative impact of renewable penetration is to increase the spinning reserves from power plants. However, involving more spinning reserves will bring additional fuel consumption, which is not an economic and energy efficient way to handle this problem.

* Corresponding author.

E-mail address: yitang@ntu.edu.sg (Y. Tang).

In order to improve system resilience and energy efficiency, demand response (DR) has been identified as an effective way in recent years [7]. In the meantime, the deregulation of the frequency regulation market has also promoted the application of DR. Typically, the DR scheme is to adjust the load demand as required by the power grid wherever necessary, which can be further classified as direct load control methods [8] and pricing based control methods for indirect load adjustment [9]. While researchers are still exploring the advanced control strategies, where the responsive loads could provide timely frequency support and balance the power and energy consumption more efficiently in modern power systems. In recent years, thermostatically-controlled loads (TCLs) such as air conditioning systems, water heaters, and refrigeration systems, have become a promising candidate for DR [10]. The increasing share of TCLs in total electrical energy consumption (especially in tropical regions like Singapore) offers great flexibility for grid ancillary services. A major difference between TCLs and conventional load shedding is that the room temperature or customers comfort level has to be taken into account. Usually, the power of a single TCL unit is quite small, so a group of TCLs should be aggregated together for practical applications. The TCL aggregator can be modeled based on bin transition models [11] and general battery models [12]. The field test has been conducted to evaluate the aggregated effects of these thermal loads in [13]. Particularly, the grid-interactive smart building (GISB), as an aggregator of TCLs, can be view as one entity from the grid perspective. Through changing the power consumption of each TCL while adjusting the temperature within the user's comfort zone, the GISB can realize an aggregated power response in the short time-scale. A GISB with controllable TCLs can function as virtual energy storage systems which could contribute actively to grid ancillary services. In this paper, how to effectively utilize GISBs for timely frequency support will be explored.

1.2. Literature survey

Previous research has demonstrated the potential of TCL aggregators/smart buildings for various system ancillary services such as primary/secondary frequency regulation [14] voltage regulation [15], load following [16], and system reserves [17]. However, it is noticed that several issues still have not been well addressed by state-of-the-art.

Firstly, the capacity from one aggregator or GISB may still be too small for supporting grid operations. In the meantime, as the development of Internet-of-Things, the number of demand-side controllable units and their aggregators keeps increasing. Therefore, it is sensible to further aggregate the GISB in a community or coordinate them at the higher control level to make a bigger impact, which leads to 'aggregator of aggregators'. Regarding the aggregation or coordination methodologies of demand-side aggregators for frequency control, it is usually achieved in two manners, i.e. centralized and distributed. In [18], the centralized secondary frequency control of TCL aggregators is investigated with an experimental case study in Denmark. In [19], a centralized hierarchical control of TCL aggregators has been proposed for primary frequency support. The limitations of the centralized approach are that the central controller suffers extensive computation and communication burdens especially when the system scale is large, and it is inherently vulnerable to single-point communication failures. An alternative approach is the distributed control scheme, which disperses computation and communication burden into the distributed controllers and is more robust to communication failures. In [20], the distributed average consensus algorithm has been applied for power allocation for the upper-layer coordination of load aggregators. In [21], a distributed leader-follower control scheme for automatic generation control by a load aggregator has been proposed. This research work is extended in [22], where the bin transition model of TCL aggregator is considered. It can be found that existing works [20–22] mainly focus on distributed power sharing among multiple load/TCL aggregators. The distributed aggregation control for multiple GISBs while considering

temperature or comfort levels sharing problem has not been fully addressed. It is also necessary to consider the comfort levels when controlling a community of GISBs for frequency regulation.

Secondly, some practical issues regarding infrastructures to implement the GISBs or demand-side aggregators for frequency regulation services are to be further considered. In a residential community, most buildings/houses may not have a frequency measurement device. As discussed in [23], the frequency measurement units are still too expensive for large scale applications in power distribution level networks, such as a community. Compared to install a new frequency measurement, the control implementation based on current communication infrastructures is a more flexible, scalable and economical choice. In this condition, a community only needs to have one leader communication node, which can measure local frequency and receive secondary control signals from grid operators. This leader node can be located at the community substation, which generates the control reference signals for all GISBs in the community. Therefore, the distributed aggregation control of GISBs has significant necessity in the residential communities.

Thirdly, different from [21] and [22], which discuss the distributed controlled load/TCL aggregators for secondary frequency control, the capability of GISBs for timely primary frequency support is investigated. The decentralized/local control is a straightforward way to deploy primary frequency regulation by demand response [24] and thermal loads [25]. However, the limitation of frequency measurement infrastructure discussed above, a community of GISBs may need to participate in the frequency support in a distributed way based on sparse communication networks. When the system frequency deviations exceed certain limits, the distributed controlled GISBs can also provide timely frequency support. In addition, the power and comfort levels can also be fairly shared among all participating GISBs, which is hard to achieve by fully decentralized control.

Besides, the distributed sliding mode control (DSMC) method is proposed to achieve the distributed aggregation control of GISBs. The DSMC, as a finite-time consensus control approach, has received increasing attention for its advantages of finite-time convergence, easy implementation and high robustness against uncertain disturbances [26]. This control method is utilized for formation control of multiple vehicles [27] and state-of-charge balancing control of multiple batteries [28]. So in this paper, it is applied to distributed aggregation control of GISBs for frequency support. The simulation results also validates it is advantageous in converge speed and withstanding time-delay over conventional linear methods.

1.3. Contributions of this paper

To fill the research gap of existing works, a new distributed aggregation control approach for multiple grid-interactive smart buildings is proposed to provide fast frequency support to the power system. Compared with previous works, the contributions of this paper are:

- (1) The practical issue of utilizing a group of GISBs in a frequency control area (e.g a community) for timely frequency support is investigated, which has rarely been addressed by state-of-the-art.
- (2) A novel aggregation control for a group of GISBs system is based on the distributed sliding mode control method. This control only relies on peer-to-peer communications and sparse networks. The stability of the proposed DSMC method is proved via the Lyapunov method.
- (3) The GISB aggregator can operate in the frequency support mode or comfort/energy recovery mode depending on area frequency deviations. The power and comfort/energy level reference for each GISB in the aggregator is calculated by a leader control.
- (4) The GISB aggregator with the proposed distributed aggregation method has both superior internal and external characteristics. Internally, fair power and comfort/energy level sharing among all

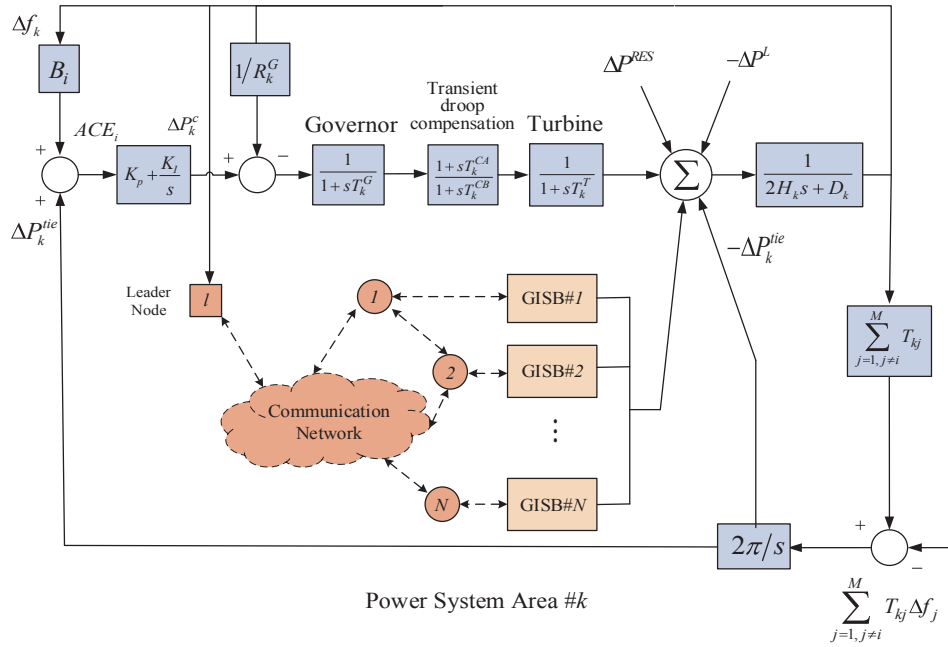


Fig. 1. An overview of the multi-area load frequency control scheme with GISBs.

participated GISBs are realized. Externally, the entire aggregator can track leader control references to achieve finite-time power tracking and comfort/energy level recovery.

- (5) The proposed method is validated in a three-area power system with multiple GISBs and RESs, considering both system contingency and normal operation scenarios. The impact of communication delay on the proposed method and comparison with the linear control method are also studied.

2. System modelling

In this paper, the GISBs in one community area is controlled as an aggregator for fast frequency support to the power system. The GISBs refer to the buildings installed with air conditioning systems for cooling. The GISBs in each area is controlled in a distributed way via a sparse communication network. An overview of the multi-area load frequency control framework with GISBs is shown in Fig. 1.

2.1. Multi-area power system with GISBs

A power system with M interconnected control areas (indexed by $k = 1, 2, \dots, M$). The multi-area power system can be represented by an undirected graph $G_p = (V_p, E_p)$, where the nodes $V_p = \{v_{p1}, v_{p2}, \dots, v_{pN}\}$ represent the control areas, and the edges $E_p \subseteq V_p \times V_p$ represent the tie-lines connecting the control areas. The topology and coupling factors of the multi-area power system are depicted by an adjacency matrix $\mathbf{T} = [T_{kj}] \subseteq \mathbb{R}^{M \times M}$, where $T_{kj} > 0$ if two areas have a tie-line connection, otherwise $T_{kj} = 0$.

The generators are controlled by primary and secondary control, while RESs power output and load demands are uncontrollable disturbances for the LFC. Based on the famous swing equation of generators [29], the power mismatch and frequency deviation in k th control area can be represented as:

$$\Delta f_k(s) = \frac{1}{2H_k s + D_k} \{-\Delta P_k^L(s) + \Delta P_k^{RES}(s) + M_k(s) \left[\Delta P_k^c(s) - \frac{1}{R_k^G} \Delta f_k(s) \right] - \Delta P_k^{tie}(s) + \Delta P_k^{agg}(s)\} \quad (1)$$

where Δf_k is the frequency deviation in i th control area, H_k, D_k, R_k^G , are

the system inertia, load damping, speed droop coefficient, respectively. $\Delta P_k^L, \Delta P_k^{RES}, \Delta P_k^{tie}$, and ΔP_k^{agg} are power variations of loads, RESs, tie-line, and aggregator of GISBs, respectively. ΔP_k^c denotes the control effort from secondary control. M_k denotes the dynamics of the generators, which is described by

$$M_k(s) = \frac{1}{1 + sT_k^G} \cdot \frac{1}{1 + sT_k^T} \cdot \frac{1 + sT_k^{CA}}{1 + sT_k^{CB}} \quad (2)$$

where T_k^G and T_k^T are the time constants of the generator and turbine. T_k^{CA} and T_k^{CB} are the time constants of a transient droop compensator [30].

The power exchange of tie-line ΔP_k^{tie} is calculated as

$$\Delta P_k^{tie}(s) = \frac{2\pi}{s} \cdot \left[\sum_{j=1}^M T_{kj} (\Delta f_k(s) - \Delta f_j(s)) \right] \quad (3)$$

In the multi-area LFC, the objective of secondary control is to eliminate the area control error (ACE), which is commonly achieved by a proportional integral (PI) controller. The ACE and PI-based secondary control are represented as

$$ACE_k(s) = B_k \Delta f_k(s) + \Delta P_k^{tie}(s) \quad (4)$$

$$\Delta P_k^c(s) = \left(K_p + \frac{K_I}{s} \right) ACE_k(s) \quad (5)$$

where B_k is the frequency bias factor. K_p and K_I are the proportional and integral gains, respectively. In practice, the frequency recovery by secondary control can be quite slow. Typically, it takes about 10–15 min for system frequency restoration [31]. It motivates us to exploit the GISBs for fast and timely frequency support.

2.2. Modeling of grid-interactive smart building

For a smart building with a number of TCLs, their aggregate behavior can be approximated by using a continuous model [12,19], which functions as a virtual energy storage system with dissipation. It is considered there are N GISBs (indexed by $i = 1, 2, \dots, N$) in each control area. The average value of internal temperature in the i th GISB can be estimated by the following differential equation:

$$C_i^{th} \dot{\theta}_i(t) = \frac{\theta^{amb}(t) - \theta_i(t)}{R_i^{th}} - \eta_i \frac{p_i(t)}{\lambda_i} + \omega_i(t) \quad (6)$$

where θ_i (°C) and θ^{amb} (°C) are the internal and ambient temperature. C_i^{th} and R_i^{th} are the thermal capacitance (kWh/°C) and thermal resistance (°C/kW). λ_i is the number of TCLs in i th GISB. $p_i \in [0, \lambda_i \bar{P}]$ is the power consumption of all air conditioners in i th GISB. η_i is the thermal coefficient, which is positive for cooling TCLs and negative for heating TCLs. ω_i is treated as a Gaussian disturbance with zero means [11]. This model provides an estimation of the average value of internal temperature in a GISB regarding its total air conditioners power consumption.

In practice, the internal temperature of each building should be kept in a customer comfort zone. Namely, each GISB should be maintained within a temperature range $[\theta^{set} - \Delta\theta, \theta^{set} + \Delta\theta]$, where θ^{set} is the nominal temperature set-point and $\Delta\theta$ is the temperature tolerance. As different buildings may have different comfort temperature ranges, they are unified into a common index between $[0, 1]$ for convenience. This index is called the *comfort level* (i. e. energy level) of a GISB, which is calculated as follows:

$$\varepsilon_i(t) = \frac{\theta_i(t) - \theta_i^{set} + \Delta\theta_i}{2\Delta\theta_i} \quad (7)$$

where the comfort level of GISB should be maintained in the range of $\varepsilon_i \in [0, 1]$.

Substituting (7) into (6), then the dynamics of comfort level can be derived as:

$$\dot{\varepsilon}_i(t) = -\frac{1}{C_i^{th} R_i^{th} \lambda_i} \varepsilon_i(t) - \frac{\eta_i}{2\Delta\theta_i C_i^{th} \lambda_i} p_i(t) + \frac{\theta^{amb}(t) - \theta^{set} + \Delta\theta_i + R_i^{th} \omega_i(t)}{2\Delta\theta_i C_i^{th} R_i^{th}} \quad (8)$$

In order to control the system (8), an auxiliary state variable $\xi_i(t)$ for feedback linearization is defined here, which is equal to the right-hand side of (8):

$$\dot{\xi}_i(t) = a_i \varepsilon_i(t) + b_i p_i(t) + d_i(t) \quad (9)$$

where a_i , b_i , and d_i represent the corresponding parameters in (9).

Differentiating $\xi_i(t)$ at both sides, a set of heterogenous second order systems representing the dynamics of GISBs can be formulated as follows:

$$\begin{cases} \dot{\varepsilon}_i(t) = \xi_i(t) \\ \dot{\xi}_i(t) = a_i \xi_i(t) + b_i u_i(t) + \dot{d}_i(t) \end{cases} \quad (10)$$

where $u_i = \dot{p}_i(t)$ is the control input to be designed in Section 3.

In addition, to maintain the comfort level of a GISB at a reference value ε^* , the GISB should consume a certain amount of power. This power consumption is defined as the *baseline power* of a GISB $p_i^{base}(t)$, which is obtained by substituting ε^* into (9):

$$p_i^{base}(t) = \lim_{t \rightarrow \infty} \frac{\xi_i(t) - a_i \varepsilon_i(t) - d_i(t)}{b_i} = \frac{-a_i \varepsilon^* - d_i(t)}{b_i} \quad (11)$$

Thus, $\sum_{i=1}^N p_i^{base}(t)$ is the baseline power for the aggregator of GISBs in one control area.

Remark 1: The comfort level of a GISB indicates the thermal ‘energy’ stored in it. In this paper, we only consider the cooling effect of the air conditioning system in tropical areas. $\varepsilon_i = 1$ means the GISB is at the highest allowable temperature, and the cooling power of the GISB cannot be further decreased. $\varepsilon_i = 0$ means the GISB is at the lowest allowable temperature, and the cooling power of the GISB cannot be further increased. The behavior of a GISB is similar to an ESS with dissipation. If the GISB is working at the baseline power defined in (9), the GISB will be maintained at the desired temperature or comfort level. If the GISB decrease its power consumption below the baseline, it functions to inject power or discharge to the grid. On the contrary, if the GISB increases its power consumption above the baseline, it functions

to absorb power or charge from the grid.

2.3. Communication network of GISBs

The communication networks can be depicted by a graph $G_B = (V_B, E_B)$, where $V_B = \{v_{B1}, v_{B2}, \dots, v_{BN}\}$ is a set of nodes and $E_B = V_B \times V_B$ is a set of edges [32]. Each node is associated with a communication agent, and edges represent communication links for data exchange. In this research, bidirectional communication links are considered, which means the graph is undirected, i.e. $(v_{Bi}, v_{Bj}) \in E_B \Rightarrow (v_{Bj}, v_{Bi}) \in E_B \forall i, j$. A matrix $A = [a_{ij}]$ is called the adjacency matrix and a_{ij} can be defined as

$$a_{ij} = \begin{cases} 1, & \text{if } (v_{Bi}, v_{Bj}) \in E_B \\ 0, & \text{otherwise.} \end{cases} \quad (12)$$

The Laplacian matrix is represented as $L = [l_{ij}]$, and the element l_{ij} is calculated from

$$l_{ij} = \begin{cases} -a_{ij}, & i \neq j \\ \sum_{i=1}^N a_{ij}, & i = j \end{cases} \quad (13)$$

In this paper, the communication network of GISBs is considered to have a *leader* (labeled as node 0) and the interaction topology is expressed by the graph \bar{G}_B . This leader–follower communication network contains original graph G_B , node v_{B0} and edges (v_{Bi}, v_{B0}) from node v_{B0} to other nodes. The leader can send information to followers, but not vice versa. The pinning matrix $G = \text{diag}\{g_i\}$ is used to describe whether each follower directly receive information from the leader, where

$$g_i = \begin{cases} 1, & \text{if } \exists (v_{Bi}, v_{B0}) \\ 0, & \text{otherwise.} \end{cases} \quad (14)$$

One important property which guarantees the convergence of a leader–follower consensus algorithm with the graph \bar{G}_B is that all the eigenvalues of matrix $L + G$ have negative real parts.

3. Proposed control framework for GISBs

The block diagram illustrates the proposed control framework, as shown in Fig. 2. In Fig. 2, the multi-area power system model is described by (1)–(5). The frequency signal of k th Area is given to the leader control of the GISB aggregator to generate the tracking references by (16)–(19). Then the reference signals are shared to each GISB through the sparse communication network \bar{G}_B given in (12)–(14). In the meantime, the information exchange of system states among adjacent GISBs is also accomplished in the communication network \bar{G}_B . With the received information, the DSMC control given in (20)–(26) will calculate the control inputs (u_1, \dots, u_N) for each GISB model. The GISB models will execute the control commands and then update the new system states to the DSMC control laws. Finally, the aggregated power of GISBs is imported to the power system model for frequency support. In the following sub-sections, the control objectives of the proposed method are introduced. The leader control, as the key linkage of the system frequency and the power consumption of GISBs, is proposed. After that, the proposed distributed sliding mode control of GISBs and its stability analysis is presented in detail.

3.1. Control objectives

The proposed control aims to utilize a group of GISBs for primary frequency support while considering users’ comfort. Three control objectives are to be met: (i) the aggregation of GISBs is able to track the power of primary frequency control in the *frequency support mode*. (ii) The comfort levels of GISBs are to be recovered to a reference value ε^* (e.g. 50%) in *comfort recovery mode* (i.e. energy recovery mode). (iii) The comfort levels of GISBs are to be gradually balanced during the operation.

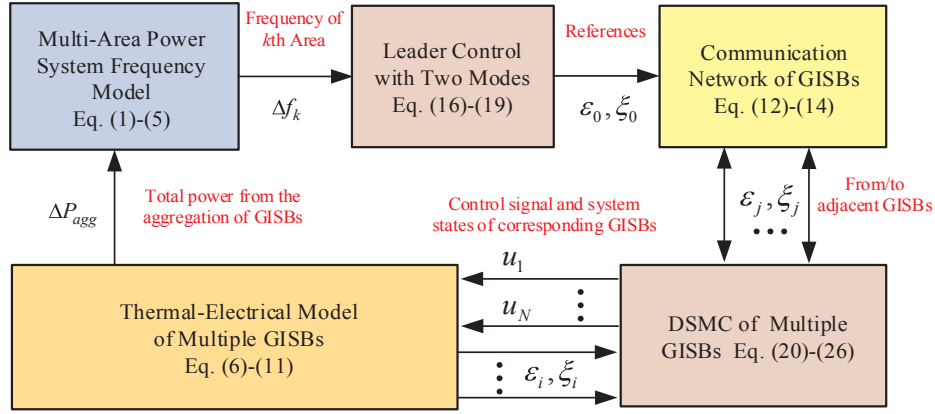


Fig. 2. Block diagram of proposed control framework.

The control problems will be solved by two steps: (i) design the leader control to update the reference states ε_0 and ξ_0 based on system frequency conditions. (ii) Design control input u_i in (10), so that system state variables ε_i and ξ_i can track ε_0 and ξ_0 via the sparse network \bar{G}_B . The following condition will be reached by the controlled system in state-state.

Consensus condition: For an aggregator of GISBs formulated by (10) with \bar{G}_B , the second-order leader-follower finite-time consensus is achieved, if for any initial states, there exists a $T_0 \in [0, \infty]$, such that

$$\lim_{t \rightarrow T_0} \|\varepsilon_i(t) - \varepsilon_0(t)\| = 0, \quad \lim_{t \rightarrow T_0} \|\xi_i(t) - \xi_0(t)\| = 0$$

$$\varepsilon_i(t) = \varepsilon_0(t), \quad \xi_i(t) = \xi_0(t), \quad \forall t \geq T_0, \quad i = 1, 2, \dots, N. \quad (15)$$

Remarks 2: In this paper, the *fair sharing* means that the power consumption is proportionally shared among GISBs with respect to their parameters, so that the comfort level is equalized during the operation. As defined in *Consensus condition* in (15), the system state variables $\varepsilon_i(t)$ and $\xi_i(t)$ in (10) will be converged to $\varepsilon_0(t)$ and $\xi_0(t)$. This also indicates that all the comfort level $\varepsilon_i(t)$ and auxiliary state variable $\xi_i(t)$ will be equalized in steady-state, i.e. $\lim_{t \rightarrow T_0} \|\varepsilon_i(t) - \varepsilon_j(t)\| = 0$, $\lim_{t \rightarrow T_0} \|\xi_i(t) - \xi_j(t)\| = 0$. In addition, the power consumption of each GISB $p_i(t)$ can be derived from (9).

3.2. Leader control of GISBs

This paper proposes two operating modes for an aggregator of GISBs: frequency support mode (FSM) which is active when system frequency is out of the acceptable range, and comfort recovery mode (CRM) when the system frequency is within the acceptable range. This is illustrated in Fig. 3.

The leader control to update the reference states ε_0 and ξ_0 is proposed to incorporate the GISB aggregator into LFC. The update rules of ε_0 and ξ_0 are different depending on the operation modes. Corresponding power will be consumed in each mode, which is further illustrated as follows:

Frequency Support Mode: When the system frequency deviation is out of the thresholds $\Delta f \notin [\Delta f, \Delta \tilde{f}]$, the operation mode is activated for primary frequency support by GISBs.

The total power consumption of the aggregator of GISBs is determined as:

$$\sum_{i=1}^N p_i(t) = \begin{cases} R^{agg}(\Delta \tilde{f} - \Delta f(t)) + \sum_{i=1}^N p_i^{base}(t), & \Delta f(t) \geq \Delta \tilde{f} \\ R^{agg}(\Delta f - \Delta f(t)) + \sum_{i=1}^N p_i^{base}(t), & \Delta f(t) \leq \Delta \tilde{f} \end{cases} \quad (16)$$

where R^{agg} is the droop gain of the aggregator. The power consumption is within $\sum_{i=1}^N p_i(t) \in [0, \sum_{i=1}^N \bar{p}_i(t)]$. As illustrated in Fig. 3, the power consumption of the aggregator in this mode is the baseline power plus/minus the certain power defined in (16). The value of baseline power can be estimated by the leader control from (9).

Remark 3: The droop control gain R^{agg} and frequency thresholds $[\Delta f, \Delta \tilde{f}]$ are user-defined parameters. The system operator can adjust the contribution of the aggregator by alternating these values. Generally, the aggregator should devote its full capacity when the system frequency deviates to the safety limits. Suppose $[\Delta \underline{f}, \Delta \bar{f}]$ is maximum allowable frequency range, therefore, R^{agg} can be selected as

$$R^{agg} \geq \min \left[\frac{-\sum_{i=1}^N p_i^{base}(t)}{\Delta \underline{f} - \Delta \bar{f}}, \frac{\sum_{i=1}^N \bar{p}_i(t) - \sum_{i=1}^N p_i^{base}(t)}{\Delta \bar{f} - \Delta \underline{f}} \right] \quad (17)$$

Therefore, in the worst condition when $f = \Delta \underline{f}$ or $f = \Delta \bar{f}$, the

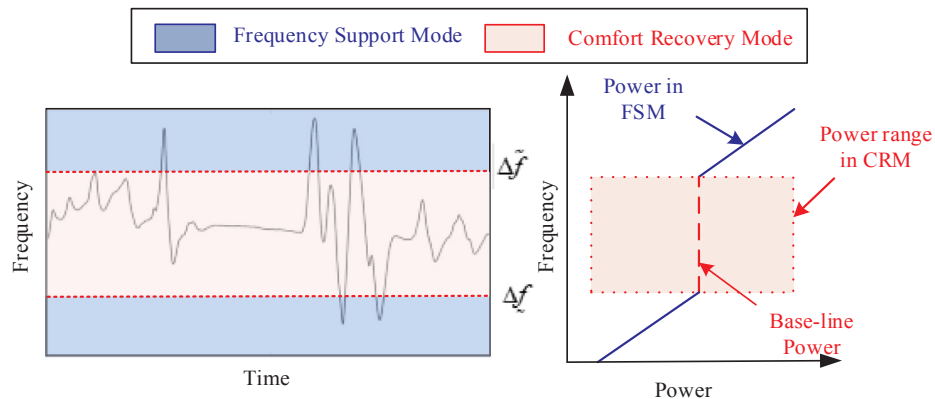


Fig. 3. Operation modes and power consumption of an aggregator of GISBs.

aggregator can provide the maximum allowable power support $\sum_{i=1}^N P_i(t) = 0$ or $\sum_{i=1}^N P_i(t) = \sum_{i=1}^N \bar{P}_i(t)$ for the system frequency support.

In steady-state, $\xi_0(t) = \xi_i(t)$, and add the right and left-hand terms of (9) from $i = 1$ to N , respectively. Thus the reference states of the leader ε_0 and ξ_0 can be obtained as:

$$\begin{cases} \xi_0(t) = \frac{\sum_{i=1}^N b_i p_i(t) + \sum_{i=1}^N [a_i \varepsilon_i(t) + d_i(t)]}{N} \\ \varepsilon_0(t) = \int_0^t \xi_0(t) dt \end{cases} \quad (18)$$

Comfort Recovery Mode: When the system frequency deviation is within the thresholds $\Delta f \in [\Delta f, \Delta \tilde{f}]$, the objective is to recover the comfort level of each GISB back to a reference value ε^* . As illustrated in Fig. 2, the power consumption of the aggregator is within a range to recover the comfort level change in frequency support mode, and the aggregator is operated at baseline power in steady-state.

The comfort recovery mode is achieved by setting the leader's reference states as:

$$\begin{cases} \varepsilon_0(t) = \varepsilon^* \\ \xi_0(t) = \dot{\varepsilon}_0(t) = 0. \end{cases} \quad (19)$$

3.3. Design of distributed sliding mode control

The sliding mode control aims to drive the system trajectory to a designed sliding mode surface based on a sliding mode control law [33]. In this section, a sliding-mode surface is designed, along which the system trajectory can meet the consensus condition (15) in finite time. Then a sliding mode control law is proposed to force the system trajectory to reach the designed sliding-mode surface in finite time for system (10) with \tilde{G}_B . As the states of agents are coupled on the sliding mode surface and the sliding mode states are decoupled out of this surface, the approach is called DSMC.

Sliding Mode Surface: The sliding mode surface should be established based on the desired control objectives. For the purpose of achieving finite-time consensus for system (10), a set of sliding mode states are represented by

$$s_i(t) = \dot{\varepsilon}_i - \sum_{j=1}^N a_{ij} [\text{sig}(\varepsilon_j - \varepsilon_i)^\alpha + \gamma \text{sig}(\xi_j - \xi_i)^\beta] - \sum_{j=1}^N g_j [\text{sig}(\varepsilon_0 - \varepsilon_i)^\alpha + \gamma \text{sig}(\xi_0 - \xi_i)^\beta] \quad (20)$$

and accordingly, the sliding mode surface is

$$\{(\varepsilon_1^T, \varepsilon_2^T, \dots, \varepsilon_N^T, \xi_1^T, \xi_2^T, \dots, \xi_N^T) | s_i = 0\} \quad (21)$$

where the function $\text{sig}(x)^\alpha = |x|^\alpha \text{sign}(x)$, $|x|$ denotes the absolute value of variable x , and $\text{sign}(\cdot)$ denotes the sign function. α, β and γ are the control gains to be selected, $\alpha \in (0, 1)$, and $\beta = 2\alpha/(1 + \alpha)$.

Sliding Mode Control Law: The sliding mode control law is designed to force the system trajectory to reach the sliding mode surface (21) in finite time. By using the sliding-mode states s_i , the control input of system (10) is controlled by the following control law:

$$u_i(t) = b_i^{-1}(u_i^{eq}(t) + u_i^{sgn}(t)) \quad (22)$$

$$u_i^{eq}(t) = \sum_{j=1}^N a_{ij} [\text{sig}(\varepsilon_j - \varepsilon_i)^\alpha + \gamma \text{sig}(\xi_j - \xi_i)^\beta] + \sum_{j=1}^N g_j [\text{sig}(\varepsilon_0 - \varepsilon_i)^\alpha + \gamma \text{sig}(\xi_0 - \xi_i)^\beta] - a_i \xi_i - \dot{d}_i \quad (23)$$

$$\dot{u}_i^{sgn}(t) = -\text{sgn}(s_i(t)) \quad (24)$$

In the designed control law only $\text{sgn}(s_i(t))$ is used rather than the exact value $s_i(t)$. Thus the calculation can be further simplified by defining a new function $g_i(t)$ as in:

$$g_i(t) = \int_0^t s_i(t) = \dot{\varepsilon}_i - \int_0^t \sum_{j=1}^N a_{ij} [\text{sig}(\varepsilon_j - \varepsilon_i)^\alpha + \gamma \text{sig}(\xi_j - \xi_i)^\beta] dt \quad (25)$$

Then, the value of $\text{sgn}(s_i(t))$ can be calculated from the following equation:

$$\text{sgn}(s_i) = \text{sgn}(g_i(t) - g_i(t - \tau)) \quad (26)$$

where τ represents a time delay. Thus, instead of knowing the exact value of s_i , only whether g_i increases or decreases is to be known.

3.4. Stability analysis

In this section, the stability of the proposed DSMC for GISBs is analyzed. The finite-time consensus condition (15) of system (10) is guaranteed based on Theorem 1 and Theorem 2 proved as follows.

Theorem 1. *If the states of system (10) can reach the designed sliding mode surface in (21), then second-order consensus can be achieved in finite time.*

Proof. Based on the sufficient condition of Theorem 1, the sliding mode control law is employed to enforce the system to achieve the sliding surface $s_i = 0$. The following system can be obtained:

$$\begin{cases} \dot{\varepsilon}_i = \xi_i, \\ \dot{\xi}_i = \tilde{u}_i, \end{cases} \quad i = 1, 2, \dots, N. \quad (27)$$

$$\begin{aligned} \tilde{u}_i(t) = \dot{\varepsilon}_i = & \sum_{j=1}^N a_{ij} [\text{sig}(\varepsilon_j - \varepsilon_i)^\alpha + \gamma \text{sig}(\xi_j - \xi_i)^\beta] + \sum_{j=1}^N g_j [\text{sig}(\varepsilon_0 - \varepsilon_i)^\alpha \\ & + \gamma \text{sig}(\xi_0 - \xi_i)^\beta] \end{aligned} \quad (28)$$

Let $\hat{\varepsilon}_i = \varepsilon_0 - \varepsilon_i$, $\hat{\varepsilon}_i = \varepsilon_0 - \varepsilon_i$, the system (24) becomes

$$\begin{cases} \dot{\hat{\varepsilon}}_i = \hat{\xi}_i \\ \dot{\hat{\xi}}_i = \hat{u}_i \end{cases}, \quad i = 1, 2, \dots, N. \quad (29)$$

$$\begin{aligned} \hat{u}_i(t) = & \sum_{j=1}^N a_{ij} [(\text{sig}(\hat{\varepsilon}_j - \hat{\varepsilon}_i)^\alpha + \gamma (\text{sig}(\hat{\xi}_j - \hat{\xi}_i)^\beta))] + g_i [(\text{sig}(\hat{\varepsilon}_i)^\alpha + \gamma (\text{sig}(\hat{\xi}_i)^\beta))] \end{aligned} \quad (30)$$

According to [28], choose a Lyapunov function as

$$V_1 = \frac{1}{2} \sum_{i=1}^n (\hat{\xi}_i)^2 + \sum_{i=1}^n \sum_{j=1}^n \int_0^{\hat{\varepsilon}_j - \hat{\varepsilon}_i} a_{ij} (\text{sig}(s)^\alpha) ds + \sum_{i=1}^n \int_0^{\hat{\xi}_i} \hat{\xi}_i (\text{sig}(s)^\alpha) ds \quad (31)$$

Take the derivative of V_1 , it can be obtained that

$$\begin{aligned} \dot{V}_1 = & \sum_{i=1}^N \hat{\xi}_i \left[\sum_{j=1}^N a_{ij} (\text{sig}(\hat{\varepsilon}_i - \hat{\varepsilon}_j)^\alpha - \gamma (\text{sig}(\hat{\xi}_i - \hat{\xi}_j)^\beta) \right. \\ & \left. - g_i (\text{sig}(\hat{\varepsilon}_i)^\alpha - \gamma \text{sig}(\hat{\xi}_i)^\beta) \right] \\ & + \frac{1}{2} \sum_{i=1}^N \sum_{j=1}^N a_{ij} (\hat{\xi}_i - \hat{\xi}_j) \text{sig}(\hat{\varepsilon}_i - \hat{\varepsilon}_j)^\alpha + \sum_{i=1}^N g_i \hat{\xi}_i \text{sig}(\hat{\varepsilon}_i)^\alpha \\ & = \sum_{i=1}^N \hat{\xi}_i \gamma \left[\sum_{j=1}^N a_{ij} \text{sig}(\hat{\xi}_i - \hat{\xi}_j)^\beta - g_i \text{sig}(\hat{\xi}_i)^\beta \right] \\ & = \frac{1}{2} \sum_{i=1}^N \sum_{j=1}^N a_{ij} (\hat{\xi}_i - \hat{\xi}_j) \text{sig}(\hat{\varepsilon}_i - \hat{\varepsilon}_j)^\alpha - \sum_{i=1}^n g_i \hat{\xi}_i \text{sig}(\hat{\xi}_i)^\beta \\ & \leq \frac{1}{2} \sum_{i=1}^N \sum_{j=1}^N a_{ij} (\hat{\xi}_i - \hat{\xi}_j) \text{sig}(\hat{\xi}_i - \hat{\xi}_j)^\beta \\ & \leq 0 \end{aligned} \quad (32)$$

According to Lyapunov's second method for stability, when V_1 is positive definite (except for original point) and $\dot{V}_1 \leq 0$ with $\dot{V}_1 = 0$, if and only if $\hat{\xi}_i = \hat{\xi}_j = 0$, $\hat{\varepsilon}_i = \hat{\varepsilon}_j = 0$, then the system will be stable. This means the system will converge to $\varepsilon_i \rightarrow \varepsilon_0$, $\xi_i \rightarrow \xi_0$ at steady-state. Thus the system (10) on surface (21) is globally asymptotically stable.

Besides, the local finite-time convergence of the system (10) on surface (21) is proved. Based on Lemma 1 (Lasalle's Invariance Principle), Lemma 2 (Finite-time stability), and definition of homogeneity

with dilation in [34], it can be obtained the system with variables $(\hat{\varepsilon}_1, \hat{\varepsilon}_2, \dots, \hat{\varepsilon}_n, \hat{\xi}_1, \hat{\xi}_2, \dots, \hat{\xi}_n)$ is homogeneous of degree $\kappa = \alpha - 1 < 0$ with dilation $(2, 2, \dots, 2, 1 + \alpha, 1 + \alpha, \dots, 1 + \alpha)$. Therefore, the system (10) on surface (21) is locally finite-time stable.

If the equilibrium of a control is globally asymptotically stable and locally finite-time convergent, then the control is globally finite-time stable. This follows the principle that globally asymptotical stability implies finite-time convergence to any given bounded neighborhood of the equilibrium. Therefore, the system (10) on surface (21) is globally finite-time stable. In other words, it can be got $\hat{\varepsilon}_i - \hat{\varepsilon}_j \rightarrow 0$, $\hat{\xi}_i - \hat{\xi}_j \rightarrow 0$, $\forall i, j = 1, \dots, N$ in finite time. This completes the proof.

Theorem 2. *The states of the second-order system (10) can reach the sliding-mode surface (21), if the sliding mode control law is designed as (22)–(24). The states of system (10) will achieve second-order consensus in finite time along the sliding-mode surface (21).*

Proof. Substituting control law (22)–(24) into the sliding mode states (20), it can be obtained that

$$\begin{aligned} s_i(t) &= a_i \xi_i + \dot{d}_i(t) + b_i u_i(t) \\ - \sum_{j=1}^N a_{ij} [\text{sig}(\varepsilon_j - \varepsilon_i)^\alpha + \gamma \text{sig}(\xi_j - \xi_i)^\beta] &- \sum_{j=1}^N g_i [\text{sig}(\varepsilon_0 - \varepsilon_i)^\alpha \\ &+ \gamma \text{sig}(\xi_0 - \xi_i)^\beta] \end{aligned} \quad (33)$$

Substituting the control law (22)–(24) into (32), it can be obtained that $s_i(t) = u_i^{\text{sgn}}(t)$, $\dot{s}_i(t) = \dot{u}_i^{\text{sgn}}(t)$.

A Lyapunov function can be established in the form of

$$V_2(t) = \frac{1}{2} \sum s_i^2(t) \quad (34)$$

Again take the derivative of V_2 , it can be obtained that:

$$\dot{V}_2(t) = \sum s_i(t) \dot{s}_i(t) = -s_i(t) \text{sgn}(s_i(t)) = -|s_i(t)| \leq 0 \quad (35)$$

It guarantees that the states of the system can reach the sliding mode surface, if the control law is designed (22)–(24). Then following Theorem 1, the second-order consensus can be achieved in finite time along the surface. This completes the proof.

4. Results and discussions

In this section, simulation studies are conducted to validate the proposed control scheme in LFC. The multi-area LFC and GISBs with the proposed control scheme are implemented in Matlab/Simulink. The topology of the test system for simulation studies is shown in Fig. 4. It is assumed that there are two aggregators of GISBs with the total power rating of 6 MW in Area 1 and 8 MW in Area 2, respectively. The power rating (in kW) of each GISB and communication graphs are also given in Fig. 4. The LFC system under consideration is a per-unit system with $S_{\text{base}} = 20$ MVA, which can also be scaled up/down in other applications. The parameters for a single TCL in GISB are given in Table 1 [11]. In simulation studies, these parameters are varied within [100%, 120%] to emulate the heterogeneous feature of each GISB. The parameters of the three-area LFC system are given in Table 2 [29]. The control parameters of the proposed method used in the following test cases are shown in Table 3. In Case 1 and Case 2, the effectiveness and performance of the proposed method are demonstrated under system contingency (step response) and normal operation (time-varying PV, load and temperature) conditions, respectively. In Case 3 and Case 4, the main purpose is to validate the advantageous of the proposed method over linear methods in the aspects of converge speed and communication delay.

4.1. Case 1: System contingency in Area 1

In Case 1, the performance of the proposed control scheme for GISBs is studied under a system contingency condition in Area 1. The initial

comfort/energy levels of all GISBs are 50% and the ambient temperature is 30 °C. A load increment of 1 MW emulates the contingency at 5 s. The simulation results, in this case, are shown in Figs. 5–8, which are illustrated as follows:

In Fig. 5, the system frequency responses under original LFC and the proposed control scheme are compared. Upon the occurrence of the disturbance at 5 s, the system frequency sharply falls down. The aggregator of GISBs switches to frequency droop mode once the frequency drop exceeds 0.1 Hz. As a result, it can be observed that the maximum frequency deviation is evidently improved from -0.46 Hz to -0.27 Hz.

In Fig. 6, the total power consumption, baseline power, energy absorption and injection of the whole GISBs aggregator in Case 1 are shown. Here the calculation of the baseline power for GISB aggregator using (11) is explained. Based on typical TCL parameters given in Table 1, the baseline power of one GISB is calculated as $p_i^{\text{base}}(t) = 140 \text{ kW}$, where $a_i = -0.25$, $b_i = -3.125 \times 10^{-3}$, $d_i = 0.5625$, and $\lambda_i = 100$. In Area 1, there are totally 12 GISBs with their parameters varies within [100%, 120%] of the typical values given in Table 1. Therefore, the baseline power of whole GISB aggregator in Area 1 can be obtained by the sum of the baseline power of each GISB, i.e. $\sum_{i=1}^N p_i^{\text{base}}(t)$, which is equal to 1.8 MW as shown in Fig. 6. The selection of R^{agg} in Area 1 is 20 MW/Hz, which is aligned with the criterion in (17), i.e. $R^{\text{agg}} \geq \min[18, 42]$ MW/Hz.

In Fig. 7, the comfort level profile of GISB-1 is shown, as the comfort levels of all GISBs are equalized in this case. Besides, the power consumption of each GISB in Area 1 is demonstrated in Fig. 8. From 5 s to 44 s, the aggregator is operating below the baseline power and ‘discharge’ to the grid for primary frequency support, as shown in Figs. 5–8. When the frequency is back to 0.1 Hz at 44 s, the aggregator starts to ‘charge’ from the grid to recover the comfort/energy level to the reference value 50%.

4.2. Case 2: Normal operation in multi-area system

In Case 2, the normal operation under half-hour PV, load demands, and ambient temperature variation (see Fig. 9) is conducted to further investigate the performance of the proposed control scheme. The three-area system shown in Fig. 4 is considered. The profiles of PV and load are scaled to 1, 1.1, and 0.9 for Area 1, 2, and 3, respectively. The PV data of 1-second resolution was measured by EPRI on June 2012 [35]. The initial comfort/energy level of each GISB in Area 2 is between [46%, 54%].

Fig. 10(a)–(c) show system frequency deviations in each control area with and without the proposed control method. In Fig. 10(a)–(c), it can be observed that frequency deviations are mitigated effectively with the proposed approach, especially for the Area 1 and Area 2 with DSMC controlled GISBs. The frequency deviations can be regulated in a safe range (± 0.2 Hz) with the 6 MW GISBs in Area 1 and 8 MW GISB in Area 2. The results prove that the proposed approach is effective for frequency support.

The power consumption and comfort/energy level profiles of each GISB in Area 2 are further shown in Fig. 11 and Fig. 12, respectively. Initially, the difference in comfort level among each GISB is large. Therefore, the energy balancing effect dominates GISB dynamics. The power sharing among each GISB is substantially influenced in order to balance comfort levels. At 380 s, the comfort levels become equalized which indicates the system reaches consensus. The power sharing becomes proportional to the parameters of GISB models. During the operation, the aggregator of GISB is able to ‘charge’ or ‘discharge’ depending on the system frequency condition. The total power consumption, baseline power, energy absorption and injection of the aggregator of GISBs in Area 2 during this process is shown in Fig. 13. The calculation of baseline power is similar to the process of Case 1. The selection of R^{agg} in Area 2 is 30 MW/Hz, which is also aligned with the criterion in (17). It should be noted that the baseline power is not a constant value due to the variations of the ambient temperature. The

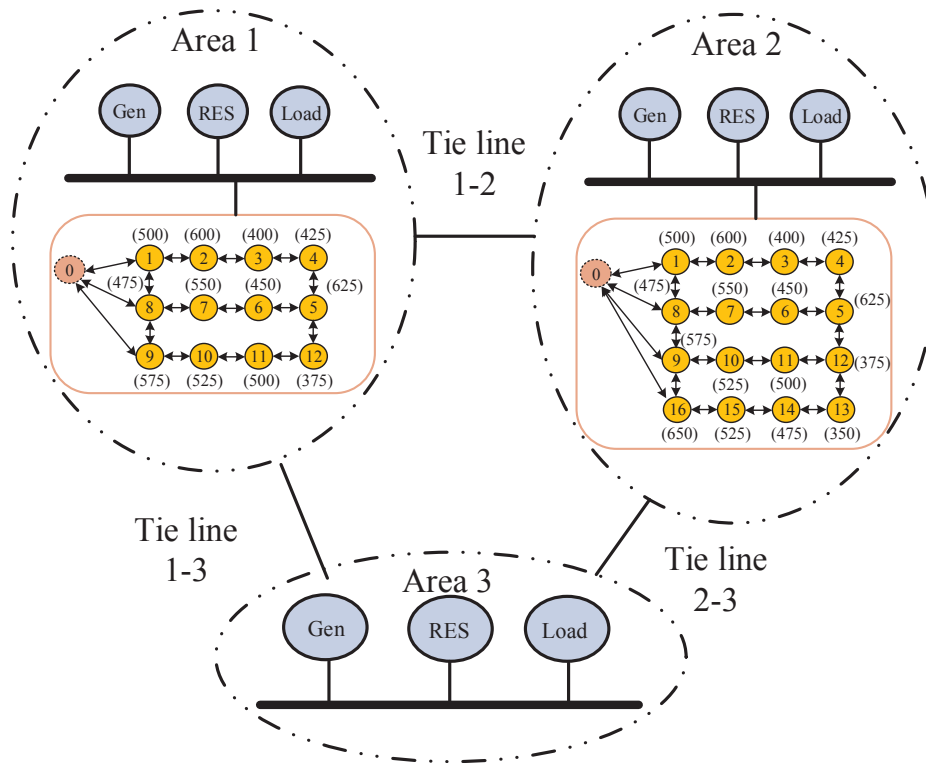


Fig. 4. The topology of the test system in the simulation studies.

Table 1
Typical parameter value for a residential TCL in GISB.

Parameter	Symbol	Value
Thermal Capacitance	C^{th}	2 kWh/°C
Thermal Resistance	R^{th}	2 °C/kW
Rated Power of an Air Conditioner	\bar{P}	5 kW
Thermal Coefficient	η	2.5
Temperature Tolerance	$\Delta\theta$	2 °C
Temperature Setpoint	θ^{set}	23 °C

Table 2
Parameters of the three-area power system.

Area No.	1	2	3
$2H$ (p.u./Hz)	0.1667	0.2	0.15
D (p.u./Hz)	0.0015	0.002	0.001
T^{CA} (s)	5	4	4.5
T^{CB} (s)	40	30	40
T^I (s)	0.3	0.2	0.25
T^G (s)	0.4	0.3	0.35
R^G (Hz/p.u.)	3	3.6	2.5
B (p.u./Hz)	0.8675	0.795	0.87
T_{ij} (p.u./Hz)	0.25	0.25	0.25
P^{agg} (MW)	6	8	0

Table 3
Parameters of the proposed control method.

Parameters	Symbols	Values
Frequency threshold	$\pm \Delta\tilde{f}$	± 0.1 Hz
Droop gain of GISB in Area 1	R^{agg}	20 MW/Hz
Droop gain of GISB in Area 2	R^{agg}	30 MW/Hz
Reference comfort level	ε^*	50%
Control gains	α, β, γ	0.8, 0.889, 0.03

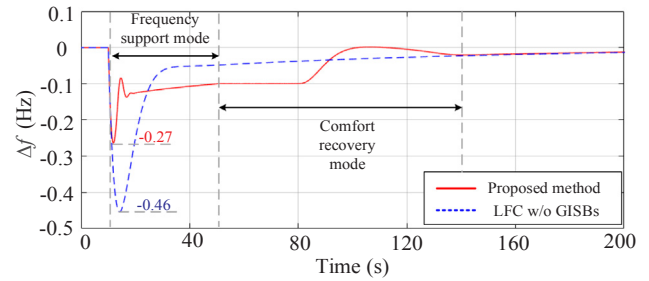


Fig. 5. Frequency response under system contingency.

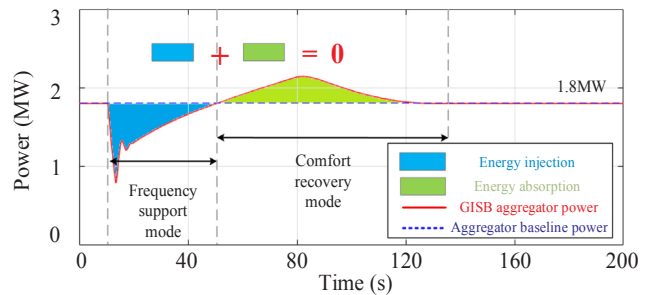


Fig. 6. Power consumption, baseline power, energy absorption and injection of the aggregator of GISBs in Area 1.

results validate that the aggregator of GISBs can operate autonomously for system frequency support under time-varying events.

4.3. Case 3: Comparison with linear consensus control

In Case 3, the proposed DSMC is compared with a traditional linear consensus control law for the second order multi-agent system proposed in [36]. Compared to the DSMC approach in this paper, the control law in [36] is ‘linear’ and ‘infinite-time’. For the GISB system considered in

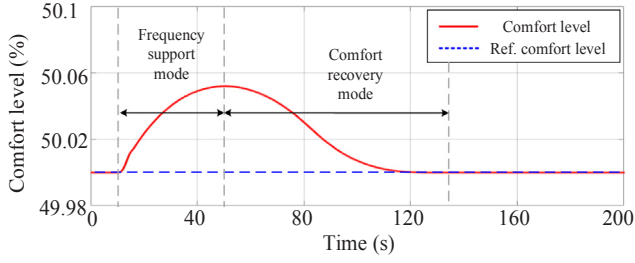


Fig. 7. Comfort/energy level of GISB-1 under system contingency.

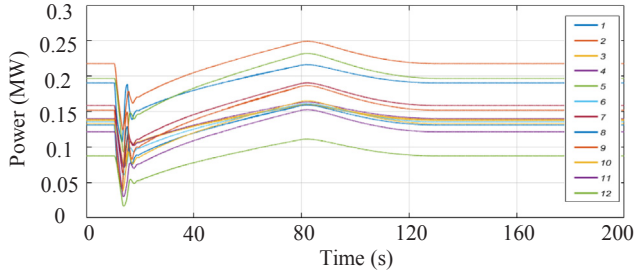


Fig. 8. Power consumption of each GISB in Area 1.

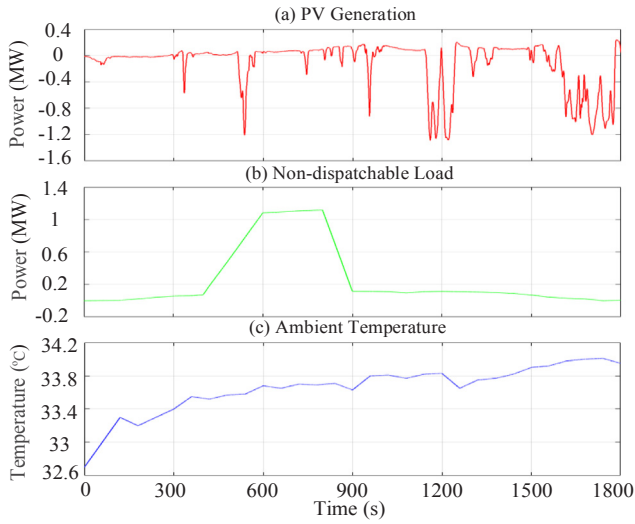


Fig. 9. PV, load demand and ambient temperature profiles of Case 2.

this paper, the linear control law can be expressed as:

$$\begin{aligned}
 u_i(t) &= k_1 \sum_{j=1}^N a_{ij} [\varepsilon_j(t) - \varepsilon_i(t) + (\xi_j(t) - \xi_i(t))] \\
 &\quad + k_2 g_i [(\varepsilon_0(t) - \varepsilon_i(t) + (\xi_0(t) - \xi_i(t))]
 \end{aligned} \quad (36)$$

where k_1 and k_2 are control gains to be selected.

To ensure a fair comparison, the same test condition in Case 2 is used and only the control law is replaced with the linear consensus control law. The same maximum power overshoot (0.44 MW of GISB-13) is kept in these two cases. As shown in Fig. 14, the maximum power overshoot is 0.44 MW, the same as in Fig. 11. However, the comfort levels in Fig. 15 converge much slower (900 s) as compared to Fig. 12 (380 s). Therefore, the proposed method can provide a faster convergence speed under the same system overshoot.

4.4. Case 4: Impact of communication Time-Delay

In Case 4, the impact of communication delay on the proposed

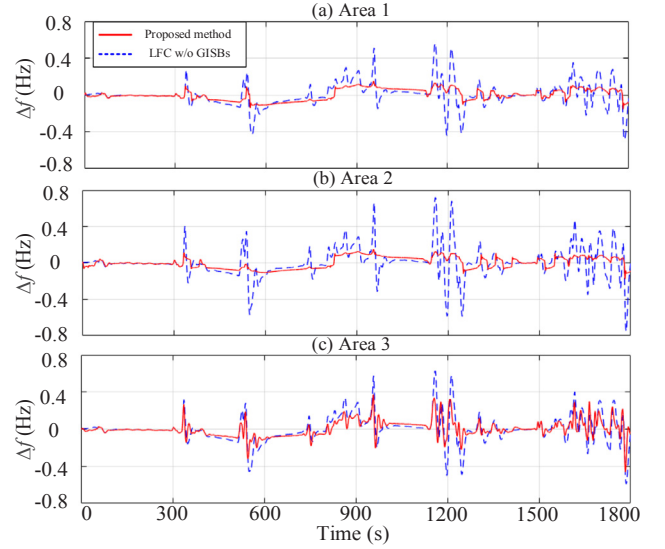


Fig. 10. Frequency deviations of each control area with and without GISBs.

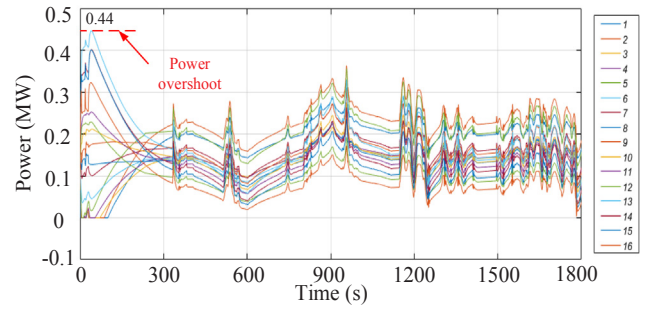


Fig. 11. Power consumption of each GISB in Area 2.

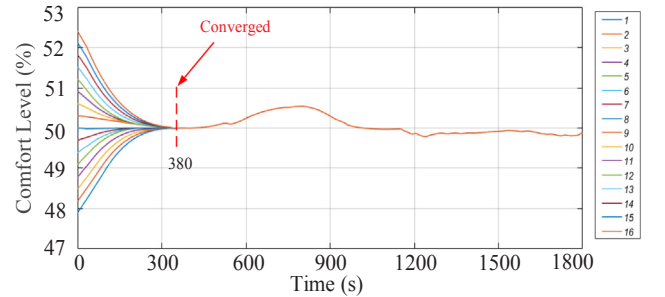


Fig. 12. Comfort/energy levels of each GISB in Area 2.

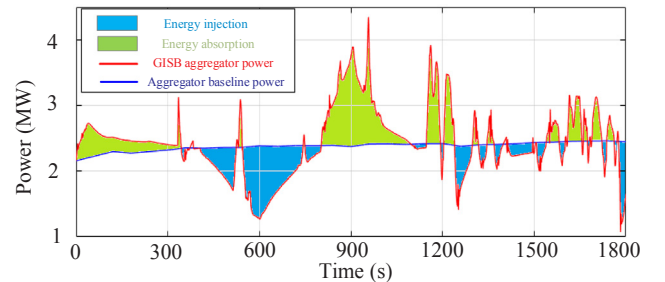


Fig. 13. Power consumption, baseline power, energy absorption and injection of the aggregator of GISBs in Area 2.

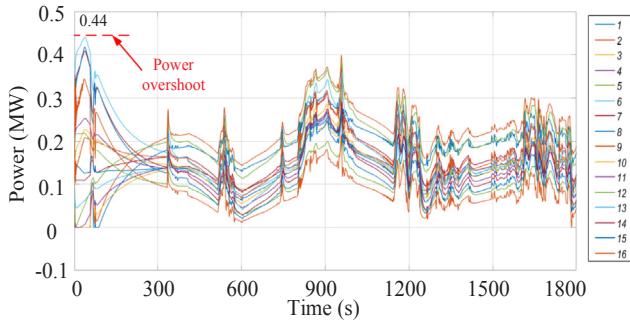


Fig. 14. Power consumption of each GISB in Area 2 with linear control law.

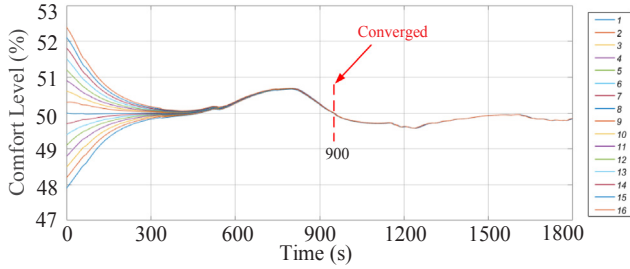


Fig. 15. Comfort levels of each GISB in Area 2 with linear control law.

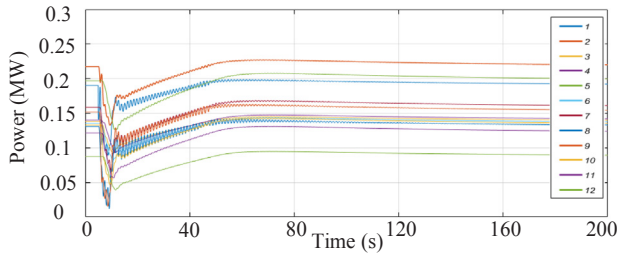


Fig. 16. Power consumption of each GISB in Area 1 with linear control law under 0.29 s delay.

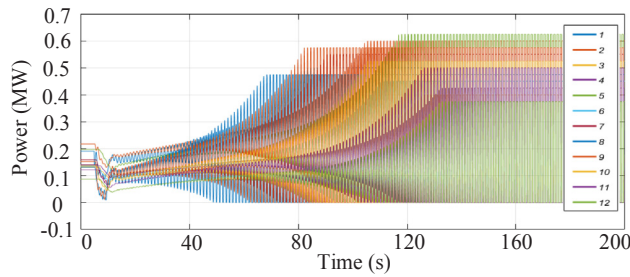


Fig. 17. Power consumption of each GISB in Area 1 with linear control law under 0.3 s delay.

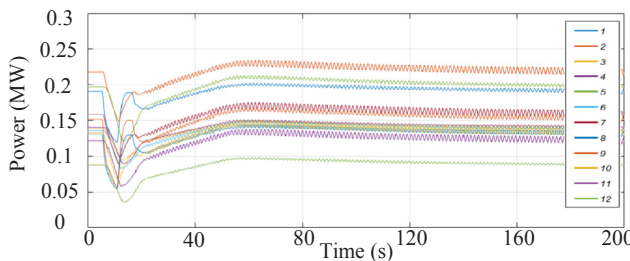


Fig. 18. Power consumption of each GISB in Area 1 with proposed control law under 0.3 s delay.

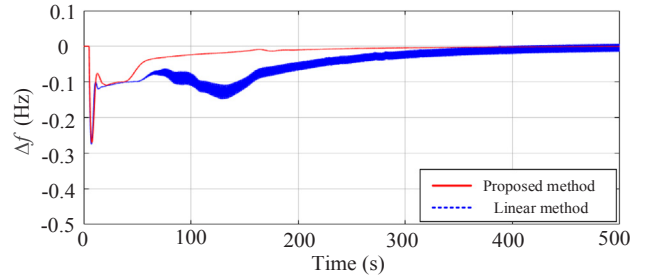


Fig. 19. Comparison of system frequency response with proposed method and linear method under 0.3 s delay.

method is further investigated. The same condition as in Case 1 is considered in this case, where the influence of network latency for GISBs in Area 1 is evaluated. First, we consider the linear control law given in (36) and let $k_1 = k_2 = 1$. Based on *Theorem 10* in [37], the upper boundary of tolerable communication delay can be estimated, which is inversely proportional to the largest eigenvalue of the matrix $(L + G)$, i.e. $\tau^* = \pi/2\lambda_{\max}(L + G)$. According to the topology of GISBs in Area 1, it can be calculated that $\lambda_{\max}(L + G) = 5.3387$ and $\tau^* = \pi/2\lambda_{\max}(L + G) = 0.2942s$. Fig. 16 and Fig. 17 shows the power consumption of each GISB with linear control law in (36) under the communication delay of 0.29 s and 0.3 s, respectively. It can be observed that the system is stable when the delay is smaller than τ^* , and the system starts to diverge when the delay is larger than τ^* . Due to the power limits of GISBs $p_i \in [0, \lambda_i \bar{p}_i]$, the power of each GISB is oscillating within its own limits. In Fig. 18, the control law is changed back to the proposed DSMC. It can be found that the proposed DSMC can tolerate the communication delay of 0.3 s with slight oscillations. Since the focus of this paper is to develop a new approach of distributed aggregation of GISBs, the upper boundary of tolerable delay is not discussed here but will be systematically considered in our future work. In Fig. 19, the frequency response of Area 1 with the proposed method and linear method ($\tau = 0.3$ s) is compared. It shows that the proposed method outperforms the linear control law given in (36) for system frequency response under large communication delay.

5. Conclusions

In this paper, multiple grid-interactive smart buildings at demand-side are utilized for timely frequency support to the power system. A new distributed sliding mode control as well as its leader control design has been proposed. The stability analysis proves the system variable can be driven to the designed sliding surface with the proposed sliding mode control law. With the proposed approach, the aggregation of grid-interactive smart buildings can provide fast frequency support while considering the comfort/energy level of each building within a community aggregator.

The proposed control scheme has been tested in a multi-area power system with renewable penetration. Simulation results have shown that the system frequency response can be improved by using the proposed method under both system contingency and normal operation conditions. The mode of operations can be changed automatically based on system frequency. The aggregation of grid-interactive smart buildings can be utilized to overcome the frequency variations. Comfort/energy level balancing and recovery can be achieved during the operation. The comparison with linear methods has been made to demonstrate the advantages of the proposed method. It is validated that the proposed method can provide fast coverage speed with stronger tolerance to the communication time-delay. In summary, the results demonstrate that the proposed aggregation method for grid-interactive smart buildings provides an effective way for fast power system frequency support.

Acknowledgement

The work in this paper is supported in part by Singtel Cognitive and Artificial Intelligence Lab for Enterprises @ NTU (SCALE Lab) and in part by Singapore Energy Innovation Research Programme Energy Storage Grant (NRF2015EWT-EIRP002-007).

References

- [1] Solar Photovoltaic System, [Online]. Available on Energy Market Authority's website https://www.ema.gov.sg/Solar_Photovoltaic_Systems.aspx.
- [2] Castro LM, Enrique A. On the provision of frequency regulation in low inertia AC grids using HVDC systems. *IEEE Trans Smart Grid* 2016;7(6):2680–90.
- [3] Shah R, Mithulananthan N, Bansal RC, Ramachandaramurthy VK. A review of key power system stability challenges for large-scale PV integration. *Renew Sustain Energy Rev* 2015;41:1423–36.
- [4] Badal FR, Das P, Sarker SK, Das SK. A survey on control issues in renewable energy integration and microgrid. *Prot Control Mod Power Sys* 2019;4(1).
- [5] Ren C, Xu Y, Zhang Y. Post-disturbance transient stability assessment of power systems towards optimal accuracy-speed tradeoff. *Prot Control Mod Power Sys* 2018;3(1).
- [6] Zhao H, Wu Q, Hu S, Xu H, Rasmussen CN. Review of energy storage system for wind power integration support. *Appl Energy* 2015;137(Jan):545–53.
- [7] Wang Q, Zhang C, Ding Y, Xydys G, Wang J, Østergaard J. Review of real-time electricity markets for integrating distributed energy resources and demand response. *Appl Energy* 2015;138(Jan):695–706.
- [8] Ng KH, Sheble GB. Direct load control—a profit-based load management using linear programming. *IEEE Trans Power Systems* 1998;13(2):688–94.
- [9] Vanthournout K, Dupont B, Foubert W, Stuckens C, Claessens S. An automated residential demand response pilot experiment, based on day-ahead dynamic pricing. *Appl Energy* 2015;155(Oct):195–203.
- [10] Patteuw D, Bruninx K, Arteconi A, Delarue E, D'haeseleer W, Helsens L. Integrated modeling of active demand response with electric heating systems coupled to thermal energy storage systems. *Appl Energy* 2015;151(Aug):306–19.
- [11] Sanandaji BM, Hao H, Poolla K. Fast regulation service provision via aggregation of thermostatically controlled loads. In: 47th Hawaii International Conference System Sciences (HICSS), 2014; Jan. 2014. p. 2388–97.
- [12] Hao H, Sanandaji BM, Poolla K, Vincent TL. Aggregate flexibility of thermostatically controlled loads. *IEEE Trans Power Syst* 2015;30(1):189–98.
- [13] Lakshmanan V, Marinelli M, Kosek AM, Nørgård PB, Bindner HW. Impact of thermostatically controlled loads' demand response activation on aggregated power: a field experiment. *Energy* 2016;94:705–14.
- [14] Maasoumy M, Sanandaji BM, Sangiovanni-Vincentelli A, Poolla K. Model predictive control of regulation services from commercial buildings to the smart grid. In: American Control Conference (ACC), 2014. IEEE; 2014.
- [15] Zakariyazadeh A, Homaei O, Jadid S, Siano P. A new approach for real time voltage control using demand response in an automated distribution system. *Appl Energy* 2014;117(Mar):157–66.
- [16] Mathieu JL, Callaway DS. State estimation and control of heterogeneous thermostatically controlled loads for load following. 2012 45th Hawaii international conference on system sciences; 2012.
- [17] Xie D, Hui H, Ding Y, Lin Z. Operating reserve capacity evaluation of aggregated heterogeneous TCLs with price signals. *Appl Energy* 2018;216(Apr):338–47.
- [18] Lakshmanan V, Marinelli M, Hu J, Bindner HW. Provision of secondary frequency control via demand response activation on thermostatically controlled loads: Solutions and experiences from Denmark. *Appl Energy* 2016;173(Jul):470–80.
- [19] Zhao H, Wu Q, Huang S, Zhang H, Liu Y, Xue Y. Hierarchical control of thermostatically controlled loads for primary frequency support. *IEEE Trans Smart Grid* 2018;9(4):2986–98.
- [20] Chen C, Wang J, Kishore SA. Distributed direct load control approach for large-scale residential demand response. *IEEE Trans Power Systems* 2014;29(5):2219–28.
- [21] Hu J, Cao J, Guerrero JM, Yong T, Yu J. Improving frequency stability based on distributed control of multiple load aggregators. *IEEE Trans Smart Grid* 2017;8(4):1553–67.
- [22] Hu J, Cao J, Yong T, Guerrero JM, Chen MZ, Li Y, et al. Demand response load following of source and load systems. *IEEE Trans Control Syst Technol* 2017;25(5):1586–98.
- [23] Dehghanpour K, Afsharnia S. Electrical demand side contribution to frequency control in power systems: a review on technical aspects. *Renew Sustain Energy Rev* 2015;41(Jan):1267–76.
- [24] Xu Z, Østergaard J, Tøgeby M. Demand as frequency controlled reserve. *IEEE Trans Power Syst* 2011;26(3):1062–71.
- [25] Trovato V, Sanz IM, Chaudhuri B, Strbac G. Advanced control of thermostatic loads for rapid frequency response in Great Britain. *IEEE Trans Power Syst* 2017;32(3):2106–17.
- [26] Guo X, Wang J, Liao F, Teo RSH. Distributed adaptive sliding mode control strategy for vehicle-following systems with nonlinear acceleration uncertainties. *IEEE Trans Vehicular Technol* 2017;66(2):981–91.
- [27] Wu Y, Li SE, Zheng Y, Hedrick JK. Distributed sliding mode control for multi-vehicle systems with positive definite topologies. In: IEEE 55th conference on decision and control (CDC), 2016. IEEE; 2016.
- [28] Morstyn T, Savkin AV, Hredzak B, Agelidis VG. Multi-agent sliding mode control for state of charge balancing between battery energy storage systems distributed in a DC microgrid. *IEEE Trans Smart Grid* 2018;9(5):4735–43.
- [29] Kundur P. Power system stability and control. New York, NY, USA: McGraw-Hill; 1994.
- [30] Cheng M, Wu J, Galsworthy SJ, Ugalde-Loo CE, Gargov N, Hung WW, et al. Power system frequency response from the control of bitumen tanks. *IEEE Trans Power Syst* 2016;31(3):1769–78.
- [31] Gauthier D, Francois B, Malarange G. Dynamic frequency control support by energy storage to reduce the impact of wind and solar generation on isolated power system's inertia. *IEEE Trans Sustain Energy* 2012;3(4):931–9.
- [32] Lewis FL, Zhang H, Hengster-Movric K, Das A. Cooperative control of multi-agent systems: optimal and adaptive design approaches. Springer Science & Business Media; 2013.
- [33] Yu W, Wang H, Cheng F, Yu X, Wen G. Second-order consensus in multiagent systems via distributed sliding mode control. *IEEE Trans Cybern* 2016;47(8):1872–81.
- [34] Wang X, Hong Y. Finite-time consensus for multi-agent networks with second-order agent dynamics. *IFAC Proc Volumes* 2008;41(2):15185–90.
- [35] 1- second resolution data, EPRI. [Online]. Available: http://dpv.epri.com/measurement_data.html.
- [36] Qiang S, Cao J, Yu W. Second-order leader-following consensus of nonlinear multi-agent systems via pinning control. *Syst Control Lett* 2010;59(9):553–62.
- [37] Olfati-Saber R, Murray RM. Consensus problems in networks of agents with switching topology and time-delays. *IEEE Trans Automatic Control* 2004;9(49):1520–33.